ChemComm

Proton-assisted activation of a Mn^{III}–OOH for aromatic C–H hydroxylation through a putative [Mn^{V}=O] species

Journal:	*ChemComm*
Manuscript ID	CC-COM-02-2024-000798.R2
Article Type:	Communication

COMMUNICATION

Proton-assisted activation of a Mn^{III}–OOH for aromatic C–H hydroxylation through a putative [Mn^{V}=O] species

Received 00th January 20xx,
Accepted 00th January 20xx

DOI: 10.1039/x0xx00000x

Sikha Gupta,[a] Parkhi Sharma,[a] Khyati Jain,[a] Bittu Chandra,[b] Sharath Chandra Mallojjala,[c,*] and Apparao Draksharapu[a,*]

Adding $HClO_4$ to the [(BnTPEN)Mn^{III}-OO]$^+$ in MeOH generates a short-lived Mn^{III}-OOH species, which converts to a putative Mn^{V}=O species. The potent Mn^{V}=O species in MeCN oxidizes the pendant phenyl ring of the ligand in an intramolecular fashion. The addition of benzene causes the formation of (BnTPEN)Mn(III)-phenolate. These findings suggest that high valent Mn species have the potential to catalyze challenging aromatic hydroxylation reactions.

Nature has primarily employed transition metals, particularly 3d metals, in the metalloenzymes as they are relatively abundant, biocompatible, and redox-active.[1-3] Among all 3d metals, iron and manganese exhibit versatile oxidation states, which nature exploits in biological catalysis to achieve many vital chemical transformations.[4-6] These include Cytochrome P450, Bleomycin, manganese superoxide dismutase (MnSOD), and catalase, to name a few.[3,5-7] Inspired by such fascinating metalloenzymes, synthetic models are being developed involving M-superoxo, M-peroxo, M-hydroperoxo, and M-oxo as active intermediates, capable of carrying out the activation of inert C-H bonds of substrates.[8,9] Bleomycin exhibits good anti-cancer activity and is recognized as a robust oxidant that initiates the cleavage of double-stranded DNA. A low spin Fe^{III}-OOH (activated Bleomycin) species is responsible for its activity.[10-12] However, synthetic nonheme, both low spin and high spin Fe^{III}-OOH complexes, on the other hand, are documented to be sluggish oxidants.[12] In contrast to iron, Mn^{III}-OOH hydroperoxo species have not been well explored as the attempts involving their formation by adding H_2O_2 to Mn^{II} complexes resulted in the formation of either Mn^{III}-(OO) species or $Mn_2^{III,IV}O_2$ dimeric species.[6,13] In contrast, iron analogs under similar conditions generate Fe^{III}-OOH species, according to the literature.[14,15] Mallart and coworkers synthesized (MeTPEN)Mn^{III} side on peroxo (MeTPEN = N^1-methyl-N^1,N^2,N^2-tris(pyridine-2-ylmethyl)ethane-1,2-diamine) complex upon the reaction of excess H_2O_2 with (MeTPEN)Mn^{II} in MeCN. Further, they proposed the formation of Mn^{III}-OOH species upon the addition of acid, however, spectroscopic evidence for the same is unavailable.[13] In 2014, Nam and coworkers reported the formation and characterization of [(14-TMC)Mn^{III}-OOH]$^{2+}$ (14-TMC = 1,4,8,11-tetramethyl-1,4,8,11-tetraazacyclotetradecane) species after the protonation of an isolated (14-TMC)Mn^{III} side on peroxo species. This [(14-TMC)Mn^{III}-OOH]$^{2+}$ species can perform electrophilic sulfide oxidation to sulphoxide.[16] Later, the same group reported [(13-TMC)Mn^{III}-OOH)]$^{2+}$ (13-TMC = 1,4,7,10-tetramethyl-1,4,7,10-tetraazacyclotridecane) species, which shows amphoteric reactivity in both electrophilic (hydrogen and oxygen atom transfer) and nucleophilic (aldehyde deformylation) reactions.[17] Recently, Lee's group reported the formation of mononuclear Mn-superoxide complexes, [(BDPP)$Mn^{III}(O_2^{\bullet-})$] (H_2BDPP = 2,6-bis((2-(S)-diphenylhy-droxylmethyl-1-pyrrolidinyl)methyl)pyridine) and [(BDPBrP)$Mn^{III}(O_2^{\bullet-})$] (H_2BDPBrP = 2,6-bis((2-(S)-di(4-bromo)phenylhydroxylmethyl-1-pyrrolidinyl)methyl)-pyridine). They assert that the Mn^{III}-superoxide complexes are capable of abstracting H atoms from 2,2,6,6-tetramethyl-1-hydroxypiperidine (TEMPO-H) to form the corresponding Mn^{III}–OOH species.[18] Jackson and coworkers demonstrated the formation of (dpaq^{2Me})Mn^{III}(OOH) species by adding H_2O_2 in the presence of $HClO_4$ to [(dpaq^{2Me})Mn^{III}(OH)]$^+$ (Hdpaq^{2Me} = 2-[bis(pyridin-2-ylmethyl)]aminoN-2-methyl-quinolin-8-yl-acetamidate) species.[19] From these studies, it is fascinating to learn how a similar species has been diverging mechanistically by minimal modifications in the ligand framework. In the present work, to synthesize a Mn^{III}-OOH intermediate, we used pentadentate BnTPEN (N^1-benzyl-N^1,N^2,N^2-tris(pyridine-2-ylmethyl)ethane-1,2-diamine) ligand frameworks. In MeOH, [(BnTPEN)$Mn^{II}(OClO_3)$]$^+$ (**1**) with H_2O_2 in the presence of Et_3N generates a (BnTPEN)Mn^{III} side on peroxo species, which upon addition of perchloric acid converts into [(BnTPEN)Mn^{III}-OOH]$^{2+}$, subsequently into a putative

[a] *Southern Laboratories-208A, Department of Chemistry, Indian Institute of Technology Kanpur, Kanpur-208016 (India). appud@iitk.ac.in*
[b] *Department of Chemistry, University of Minnesota, Minneapolis, Minnesota 55455, United States.*
[c] *Department of Chemistry, Binghamton University, Binghamton, New York 13902, United States. sharathc@binghamton.edu*
‡ *Electronic supplementary information (ESI) available: Detailed experimental procedures, characterization data, DOI: …*

$[(BnTPEN)Mn^{V}=O]^{3+}$ species. The potent $[(BnTPEN)Mn^{V}=O]^{3+}$ species is highly reactive and can oxidize MeOH into formaldehyde. Surprisingly, switching the solvent to MeCN resulted in the hydroxylation of the pendant phenyl ring of the BnTPEN ligand. The hydroxylation of the pendant ring is not favored in the presence of external substrates such as thioanisole, xanthene, MeOH, and benzene. The current study demonstrates the key reactivity of a putative $[Mn^{V}=O]^{3+}$ and its generation from a Mn^{III}-OOH species.

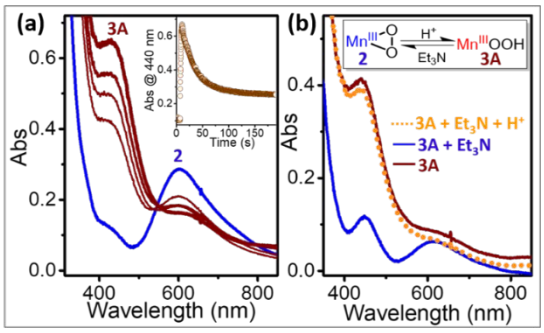

Fig. 1. (a) UV/Vis absorption spectral changes showing the formation of **3A** upon adding 10 eq. of $HClO_4$ to **2** in MeOH at -40 °C. Conditions to generate **2**: 1 mM **1** in MeOH + 2 eq. of Et_3N + 10 eq. of H_2O_2 at room temperature. (inset) The decay profile of **3A** followed at 440 nm with time. (b) UV/Vis absorption spectral changes show acid-base equilibrium between **2** and **3A**.

1 was synthesized by using our previously reported procedure.[20] According to the reported literature, the suitable way of generating Mn^{III}-OOH is via the protonation of Mn^{III}-(OO) species.[4] We prepared $[(BnTPEN)Mn^{III}\text{-}(OO)]^{+}$ species, by the treatment of **1** with 10 eq. of H_2O_2 and 2 eq. of Et_3N in MeOH, which resulted in a blue-colored species (**2**) (Fig. 1 and S1). A similar absorption spectrum was reported for $[(MeTPEN)Mn^{III}\text{-}(OO)]^{+}$ in MeCN at -25 °C.[13] In addition, ESI-MS studies on the formed species **2** revealed a signal at m/z = 510.17 with the formulation of $[(BnTPEN)Mn^{III}O_2]^{+}$, confirming its presence in the solution (Fig. S1-S5). Based on the similarities in the UV/Vis spectrum of $[(MeTPEN)Mn^{III}\text{-}(OO)]^{+}$ along with ESI-MS data, we assigned 600 nm species to be a $[(BnTPEN)Mn^{III}\text{-}(OO)]^{+}$ (**2**) species. The addition of 10 eq. of $HClO_4$ to **2** in MeOH at -40 °C generated a short-lived species **3A** with an absorption band at 420 nm, which decayed in 40 s with $t_{1/2}$ of 15 s (Fig. 1a and S6). The observed 440 nm band is closely related to the absorption spectrum of $[(14\text{-}TMC)Mn^{III}\text{-}OOH]^{2+}$, which shows a band at 384 nm.[16] Interestingly, addition of 4 eq. of Et_3N to **3A**, leads to the formation of **2**, which reverts to **3A** upon adding $HClO_4$. The presence of acid-base equilibrium between **3A** and **2** (Fig. 1b and S7) adds to our understanding of assigning the 440-nm species to be a $[(BnTPEN)Mn^{III}\text{-}OOH]^{2+}$ (**3A**). A similar observation was reported by Nam and coworkers, where $[(13\text{-}TMC)Mn^{III}\text{-}(OO)]^{+}$ and $[(13\text{-}TMC)Mn^{III}\text{-}OOH]^{2+}$ exhibited acid-base equilibrium.[17] The transient nature of **3A** in the present case restricts its analysis via ESI-MS and resonance Raman studies. Additionally, trapping **3A** using NMR spectroscopy proved challenging at -40 °C. Despite this, very weak yet distinct paramagnetically shifted signals were observed for **3A**, is consistent with the Mn oxidation state of +3 (Fig. S8). Given the instability of **3A**, even at a lower temperature of -60 °C, it probably suggests its reaction with MeOH. Favorably, the presence of formaldehyde in the decayed solution of **3A** further strengthens our hypothesis (Fig. S9).[21] Additionally, when CD_3OD was used to generate **3A**, a kinetic isotope effect of 2.2 was observed (Fig. S10), suggesting the hydrogen atom abstraction involved in the reaction.

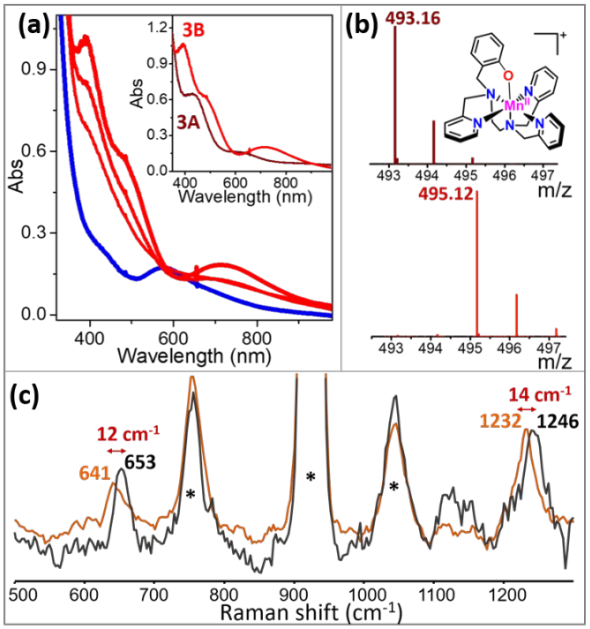

Fig. 2. (a) UV/Vis absorption spectral changes showing the formation of **3B** upon adding 10 eq. $HClO_4$ to **2** in MeCN at -40 °C. Conditions to generate **2**: 1 mM **1** in MeCN + 2 eq. of Et_3N + 10 eq. of H_2O_2 at RT. *Inset*: UV/Vis absorption spectra of **3A** (brown) and **3B** (red). (b) ESI-MS analysis of **3B** (top) and **^{18}O- 3B** (bottom) in MeCN. (c) Resonance Raman spectra of **3B** in MeCN using λ_{exc} = 405 nm at -40 °C. * Indicate solvent peaks.

To increase the stability of **3A**, we shifted the solvent system from MeOH to MeCN. Firstly, we synthesized **2** by reacting 10 eq. of H_2O_2 and 2 eq. of Et_3N with **1** in MeCN at room temperature (Fig. S11). Upon adding 10 eq. of $HClO_4$ to **2** in MeCN at -40 °C distinct from **3A**, a stable orange-colored species formed, with absorption bands at 400 nm ($\varepsilon_{400\ nm}$ = 1000 $M^{-1}cm^{-1}$), 480 nm ($\varepsilon_{480\ nm}$ = 580 $M^{-1}cm^{-1}$), and 720 nm ($\varepsilon_{720\ nm}$ = 180 $M^{-1}cm^{-1}$) (Fig. 2a and S12). In the first instance, the change in the absorption spectrum by switching the solvent from MeOH to MeCN could be thought of due to the solvatochromic effect. Surprisingly, no evidence of an acid-base equilibrium was found with **2** in this case, suggesting the formation of a different species in MeCN, which we labeled as **3B**. **3B** is unstable at room temperature and decays over time to a colorless species (Fig. S13). Surprisingly, upon varying the condition from MeCN to 1:1 or 9:1 MeCN/MeOH (vol/vol) mixtures, the species formed was **3A**, not **3B** (Fig. S14 and S15). These studies suggest that MeOH favors the formation of 440 nm species (**3A**) over **3B**. Besides, adding MeOH to **3B** did not cause any changes in the absorption band, further indicating the inability of **3B** to oxidize MeOH. We further tested the formation of the transient intermediates **2**, **3A**, and **3B** in water. Treatment of **1** in water with 10 eq. of H_2O_2 and 5 eq. of Et_3N resulted in **2** at room temperature (Fig. S16). Further addition of 20 eq. of $HClO_4$ at 5 °C generates **3B** not **3A** (Fig. S16) like the chemistry observed in MeCN.

Positive mode ESI-MS analysis of **3B** depicted signals at m/z values of 493.16 and 593.12, which are formulated as $[(BnTPEN\text{-}O)Mn^{II}]^{+}$ and $[(BnTPEN\text{-}OH)Mn^{II}(ClO_4)]^{+}$, respectively (Fig. 2b and S17). The signals shifted to two mass units, *i.e.*, m/z values of 495.16 and 595.12, when $H_2{}^{18}O_2$ was used (Fig. 2 and S18). The mass and isotopic pattern suggested the hydroxylation of the pendant phenyl ring on the BnTPEN ligand (Fig. 2). However, the strong chromophoric nature of **3B** indicates its formulation as $[(BnTPEN\text{-}O)Mn^{III}]^{2+}$.[22] Mn(III) reduction to Mn(II) might occur during mass data acquisition due to its inherent instability. **3B** exhibited sharp paramagnetically shifted NMR signals in the range of -50 to 100 ppm, resembling those of the $(BnTPEN)Mn^{III}\text{-}O\text{-}Ce^{IV}$ species, indicating the +3 oxidation state of Mn in **3B** (Fig. S19).[20] This notable change could be attributed to the presence of coordinated phenolate, leading to a stronger coupling between the manganese electron spin and the phenolate protons. However, the decayed sample of **3B** exhibited no signals due to the faster relaxation of Mn^{II} species (Fig. S19), which is in line with our ESI-MS analysis. ESI-MS data on the decayed sample of **3A** in MeOH did not show signals indicating the ligand's hydroxylation. The resonance Raman (rR) spectrum of **3B** shows two resonantly enhanced signals at 653 cm^{-1} and 1246 cm^{-1}, which shifted to 641 and 1232, respectively, upon using $H_2{}^{18}O_2$ (Fig. 2c). Que and coworkers recently reported the hydroxylation of the pendant benzyl ring of BnTPEN ligand, *i.e.*, $[(BnTPEN\text{-}O)Fe^{III}]^{2+}$, upon the treatment of Bronsted acid with $[(BnTPEN)Fe^{III}\text{-}OOH]^{2+}$ through a putative $[Fe^{V}{=}O]^{3+}$ species in MeCN at -40 °C.[23] The reported rR signal at 600 cm^{-1} is attributed to Fe—O mode, and 1100-1600 cm^{-1} signals correspond to phenolate ring deformation modes.[23] In the current study, the signal at 653 cm^{-1} is assigned to Mn^{III}—O stretch, and 1246 cm^{-1} has been assigned to C—O stretch of bound phenolate moiety. Thus, ESI-MS, resonance Raman analysis, and literature precedence support the hydroxylation of the pendant benzyl ring of the BnTPEN ligand in MeCN.

In addition, no intramolecular ligand hydroxylated product was observed when we used external substrates such as benzene, thioanisole, xanthene, etc. The product analysis of thioanisole and xanthene was carried out using mass spectrometry, and thioanisole oxide and xanthone were observed as products (Fig. S20-S23). When benzene is added as a substrate to **2**, followed by adding $HClO_4$ in MeCN at -40 °C led to the formation of a distinct band at 390 nm ($\varepsilon_{390\ nm}$ ~ 1400 M^{-1} cm^{-1}) (Fig. S24 and S25). The rR data of 390 nm species depicted multiple bands between 1650 and 500 cm^{-1} (Fig. S24). Usage of benzene-d6 shifted all the bands to lower wavenumbers compared to benzene, suggesting that their origin is from the manganese bound benzene derived oxidized product, *i.e.*, $(L)Mn^{III}$-OPh (390 nm species).[22]

However, there was no evidence of pendant benzyl ring hydroxylation in MeOH. In addition, the presence of external substrates such as benzene, thioanisole, and xanthene did not alter the chemistry observed in MeOH. To corroborate the current study, we have carried out $[(BnTPEN)Fe^{III}\text{-}OOH]^{2+}$ reaction with acid in MeOH. To our surprise, the treatment of $[(BnTPEN)Fe^{III}\text{-}OOH]^{2+}$ in MeOH with 1 eq. of $HClO_4$ caused its decay (Fig. S26), without the formation of a band at 600 nm, typical for $[(BnTPEN\text{-}O)Fe^{III}]^{2+}$ species.[23] This experiment showed that no hydroxylation of the ligand occurs in the presence of MeOH, similar to the present study. From all these experiments, we concluded that in MeCN, a potent $Mn^{V}{=}O$ species is generated upon the reaction of **2** with acid, which can hydroxylate the pendant phenyl ring of the ligand BnTPEN (in the absence of MeOH and substrates). However, in the presence of MeOH, the same reaction yields formaldehyde due to MeOH's ease of oxidation.

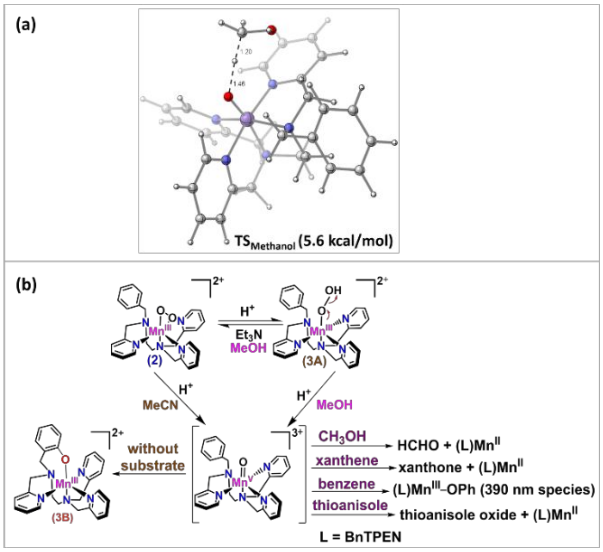

Fig. 3 (a) Computed TS and the free energy barrier for the HAT step involving the putative $Mn^{V}{=}O$ species and methanol. (b) Mechanistic pathway of the formation of putative $[Mn^{V}{=}O]^{3+}$ from $[Mn^{III}\text{-}OOH]^{2+}$ species in MeOH and MeCN at -40 °C.

This was further supported by computational modeling of key transition states (TS) involving the putative $Mn^{V}{=}O$ intermediate. B3LYP[24,25] functional with Grimme's D3 dispersion and Becke-Johnson correction was paired with def2-SVP basis set and polarized continuum model with acetonitrile as the solvent was used for these optimizations. $Mn^{V}{=}O$ geometries were also optimized across different electronic states at the same level of theory. Single point corrections were performed at B3LYP-D3(BJ)/6-311+G(d,p)[26] level of theory, and free energy corrections were performed using quasi rigid rotor harmonic oscillator approximation. Isotope effects were predicted using Paneth's isoeff code[27] with Wigner tunneling corrections. To probe the effects of methanol on $Mn^{V}{=}O$ species, TS search for the hydrogen atom transfer (HAT) step ($TS_{Methanol}$, Fig. 3a) was located at the aforementioned level of theory. This TS was energetically accessible and has a barrier of only 5.6 kcal/mol compared to the separated reactants ($Mn^{V}{=}O$ and methanol). Furthermore, the predicted k_H/k_D for this TS was found to be 2.69 and is in good agreement with the experimental value of 2.2. These two observations support a

facile HAT step acting as the quench step for Mn^{V}=O species in the presence of methanol.

Figure 3b summarizes the reaction of Mn^{III}-OO (**2**) with $HClO_4$ in methanol and acetonitrile. In methanol, the reaction of **2** with acid produces a transient Mn^{III}-OOH (**3A**) species that exhibits acid-base equilibrium with **2**. Analysis of the resultant reaction mixture revealed the formation of formaldehyde due to the oxidation of methanol. However, in acetonitrile, a distinct species **3B**, which is the product of intramolecular hydroxylation of the pendant phenyl ring, occurs. It is worth noting that the $[(BnTPEN)Mn^{IV}=O]^{2+}$ species in TFE is incapable of oxidation pendant phenyl ring and external benzene even in the presence of $HClO_4$ (Fig. S27 and S28). Similarly, the $(BnTPEN)Mn^{IV}$-OH species generated upon the addition of $HClO_4$ to the $(BnTPEN)Mn^{III}$-O-Ce^{IV} complex in MeCN is also not capable of conducting the aromatic hydroxylation reaction (Fig. S29).[20] Furthermore, the potential formation of hydroxyl radicals through homolytic cleavage of Mn^{III}-OOH is ruled out by employing terephthalic acid as a radical trap (Fig. S30).[28] Finally, TS search on the benzyl group of BnTPEN yielded two mechanistic alternatives, viz. (i) A direct HAT (TS_{HAT}) followed by a barrierless radical recombination (ii) A S_{RN1} type attack of oxygen on the benzyl group of BnTPEN (TS_{SRN1}), followed by a HAT step (TS_{HT}) as shown in SI (Fig. S31). Unsurprisingly, the direct HAT transition state was found to be unfavorable compared to TS_{SRN1} by 10.9 kcal/mol owing to hard to oxidize aromatic C-H bonds. The lack of easily oxidizable methanol altered the reaction to proceed via an S_{RN1} type pathway leading to the decay of Mn^{V}=O, lending credence to our hypothesis that the intramolecular aromatic hydroxylation in the present work can be intercepted by external substrates like MeOH, benzene, thioanisole, xanthene, etc. A putative $[Mn^{V}=O]^{3+}$ is proposed to be responsible for the observed reactivity. However, all our attempts to trap the high valent $[Mn^{V}=O]^{3+}$ species have been unsuccessful thus far. Our proposal is further strengthened by its parallel reaction with $[(BnTPEN)Fe^{III}\text{-}OOH]^{2+}$ and $HClO_4$, where similar reactivity is witnessed.[23] The current study highlights the similarities of high valent $[(BnTPEN)Mn^{V}=O]^{3+}$ and $[(BnTPEN)Fe^{V}=O]^{3+}$ species within the same ligand systems and thereby augmenting our comprehension of their reactivities.

The work presented here is financially supported by SERB (CRG/2023/001112), and CSIR (01(3050)/21/EMR-II) is greatly acknowledged. Computational support was provided through the ACCESS program, which is supported by the National Science Foundation grants #2138259, #2138286, #2138307, #2137603, and #2138296 utilizing allocations and CHE210031 (M.S.C.). We thank Prof. C. V. Sastri and Mr. Jagnyesh K. Satpathy for their assistance with the EPR experiments. We are thankful to Dr. Dharmaraja Allimuthu and Ms. Sathyapriya Senthil for their assistance with HPLC analyses. AD is thankful to Prof. Lawrence Que, Jr., for low-temperature NMR experiments.

Conflicts of interest

There are no conflicts to declare.

Notes and References

1 W. Keown, J. B. Gary and T. D. P. Stack, *J. Biol. Inorg. Chem*., 2017, **22**, 289–305.
2 S. Hong, Y. M. Lee, K. Ray and W. Nam, *Coord. Chem. Rev.*, 2017, **334**, 25–42.
3 M. Guo, T. Corona, K. Ray and W. Nam, *ACS Cent. Sci*., 2019, **5**, 13–28.
4 D. B. Rice, A. A. Massie and T. A. Jackson, *Acc. Chem. Res*., 2017, **50**, 2706–2717.
5 C. M. Krest, E. L. Onderko, T. H. Yosca, J. C. Calixto, R. F. Karp, J. Livada, J. Rittle and M. T. Green, *J. Biol. Chem*., 2013, **288**, 17074–17081.
6 K. P. Bryliakov and E. P. Talsi, *Coord. Chem. Rev.,* 2014, **276**, 73–96.
7 I. G. Denisov, T. M. Makris, S. G. Sligar and I. Schlichting, *Chem. Rev*., 2005, **105**, 2253–2277.
8 T. M. Makris, K. von Koenig, I. Schlichting and S. G. Sligar, *J. Inorg. Biochem*., 2006, **100**, 507–518.
9 A. A. Shteinman, *Russ. Chem. Bull*., 2001, **50**, 1795–1810.
10 M. Lubben, A. Meetsma, E. C. Wilkinson, B. Feringa and L. Que Jr., *Angew. Chem. Int. Ed.*, 1995, **34**, 1512–1514.
11 A. J. Simaan, S. Döpner, F. Banse, S. Bourcier, G. Bouchoux, A. Boussac, P. Hildebrandt and J. J. Girerd, *Eur. J. Inorg. Chem.*, 2000, 1627–1633.
12 W. Nam, *Acc. Chem. Res.,* 2015, **48**, 2415–2423.
13 S. Groni, P. Dorlet, G. Blain, S. Bourcier, R. Guillot and E. Anxolabéhère-Mallart, *Inorg. Chem*., 2008, **47**, 3166–3172.
14 J. Serrano-Plana, F. Acuña-Parés, V. Dantignana, W. N. Oloo, E. Castillo, A. Draksharapu, C. J. Whiteoak, V. Martin-Diaconescu, M. G. Basallote, J. M. Luis, L. Que Jr., M. Costas and A. Company, *Chem. A Eur*. J., 2018, **24**, 5331–5340.
15 S. Kal, A. Draksharapu and L. Que Jr*., J. Am. Chem. Soc*., 2018, **140**, 5798–5804.
16 H. So, Y. J. Park, K. Bin Cho, Y. M. Lee, M. S. Seo, J. Cho, R. Sarangi and W. Nam, *J. Am. Chem. Soc*., 2014, **136**, 12229–12232.
17 M. Sankaralingam, Y. M. Lee, S. H. Jeon, M. S. Seo, K. Bin Cho and W. Nam, *Chem. Commun*., 2018, **54**, 1209–1212.
18 Y. H. Lin, H. H. Cramer, M. Van Gastel, Y. H. Tsai, C. Y. Chu, T. S. Kuo, I. R. Lee, S. Ye, E. Bill and W. Z. Lee, *Inorg. Chem.,* 2019, **58**, 9756–9765.
19 E. N. Grotemeyer, J. D. Parham and T. A. Jackson, *Dalt. Trans*., 2023, **52**, 14350–14370.
20 S. Gupta, P. Arora, R. Kumar, A. Awasthi, B. Chandra, R. Eerlapally, J. Xiong, Y. Gou, L. Que Jr., A. Draksharapu, *Angew. Chem. Int. Ed*., 2024, **63**, e20231637.
21 T. Nash, *Nature*, 1952, **170**, 976.
22 A. D. Andos, A. J. Bortoluzzi, M. S. B. Caro, R. A. Peralta, G. R. Friedermann, A. S. Mangrich and A. Neves, *J. Braz. Chem. Soc.*, 2006, **17**, 1540-1550.
23 S. Xu, A. Draksharapu, W. Rasheed and L. Que, Jr*., J. Am. Chem. Soc.* 2019, **141**, 16093−16107.
24 A. D. Becke, *J. Chem. Phys.*, 1993, **98**, 5648-5652
25 C. Lee, W. Yang, and R.G. Parr*, Phys. Rev. B*, 1988, **37**,785-789.
26 M. J. Frisch, J. A. Pople, and J. S. Binkley, *J. Chem. Phys.*, 1984, **80**, 3265-3269.
27 V. Anisimov, and P. Paneth, *J. Math. Chem.* 1999, **26**, 75-86.
28 V. Vyas, V. Kumar and A. Indra, Chem. Commun., 2024, **60**, 2544-2547.

